Spallation reactions in ^{27}Al and ^{56}Fe induced by 800 MeV protons

H. Vonach, A. Pavlik, and A. Wallner
Institut für Radiumforschung und Kernphysik, Universität Wien, Boltzmanngasse 3, A-1090 Wien, Austria

M. Drosg
Institut für Experimentalphysik, Universität Wien, Strudlhofgasse 4, A-1090 Wien, Austria

R. C. Haight and D. M. Drake
Los Alamos National Laboratory, P-23, MS H803, Los Alamos, New Mexico 87545

S. Chiba
Japan Atomic Energy Research Institute, Tokai-mura, Naka-gun, Ibaraki-ken 319-11, Japan
(Received 3 September 1996)

Spallation of ^{27}Al and ^{56}Fe by 800 MeV protons was investigated at the WNR facility of the Los Alamos National Laboratory. Production cross sections for a considerable number of residual nuclei were determined for both targets by use of three different methods. Because of the specific time structure of the WNR beams it was possible to observe both the prompt γ radiation resulting from the final stage of the spallation reaction and the γ radiation due to the decay of short-lived residual nuclei by delayed γ-ray spectroscopy. The activity of long-lived residual nuclei was measured several weeks after the irradiation with a calibrated high-purity Ge γ-ray detector. In the prompt γ-ray spectrum it was possible to observe the transitions from the first excited 2^+ state to the ground state for all even-even nuclei strongly populated in the spallation reactions and, from these data, to deduce the production cross sections of these mostly stable nuclei in addition to the short- and long-lived residual nuclei mentioned before. In this way production cross sections for 36 nuclides from the proton interactions with ^{56}Fe and for 12 nuclides in the case of ^{27}Al could be measured; in addition, meaningful upper limits were obtained for a number of further nuclides in both cases. The results are in reasonable agreement with previous measurements obtained by different methods; for a number of nuclides, production cross sections were determined for the first time. The present data as well as the results of all previous measurements are compared with the predictions of the semiempirical systematics and with quantum molecular dynamics calculations. [S0556-2813(97)03305-0]

PACS number(s): 25.40.Sc, 25.40.−h, 24.10.Lx

I. INTRODUCTION

The mass and charge distribution of the reaction products from spallation reactions induced by protons in the energy range from several hundred MeV to several GeV has been investigated in a number of experiments [1]. Cross sections for the formation of radioactive residual nuclei with half-lives exceeding some hours have been investigated in a number of experiments by conventional γ-ray spectroscopy and accelerator mass spectrometry (AMS) [1]. In addition, the production of stable isotopes of noble gases has been measured by gas production measurements and mass analysis [1]. Much less information, however, exists about the production of stable isotopes from elements other than noble gases, and for short-lived residual nuclei. Only one experiment has been reported for nuclides heavier than oxygen, in which the full mass and charge distribution of the spallation products has been measured by detection of the recoiling nuclei in so-called inverse kinematics at $E=600$ MeV for a wide range of target nuclei [2]. Although the results of this experiment are in reasonable overall agreement with the above-mentioned activation, AMS, and gas production measurements, there are a number of discrepancies exceeding experimental errors [1].

For the latter reason an experiment was performed using in-beam γ-ray spectroscopy. This method, which so far has not been used in the study of spallation reactions, allows the determination of cross sections for formation of stable and very short-lived isotopes, both of which cannot be measured by conventional activation techniques. In addition it is the purpose of this paper to demonstrate that in-beam γ-ray spectroscopy can be used successfully for spallation studies of light- and medium-weight nuclei in spite of the extreme complexity of the prompt γ-ray spectra, which are a superposition of the γ cascades from a large number of residual nuclei.

Two nuclei, ^{27}Al and ^{56}Fe have been selected for this study because they have been studied before in a number of papers [1,2]. Thus these nuclei are well suited for the goal of obtaining a rather complete mass and charge distribution of the residual nuclei by combining our results with the existing data base. In addition, checks of the results obtained by very different methods become possible for a number of residual nuclei.

In Secs. II and III we describe the experiments and the data analysis. In Sec. IV we present the results, the formation cross section for a large number of residual nuclei by proton-induced spallation of ^{27}Al and ^{56}Fe and compare them to the existing data and to the prediction of the semiempirical sys-

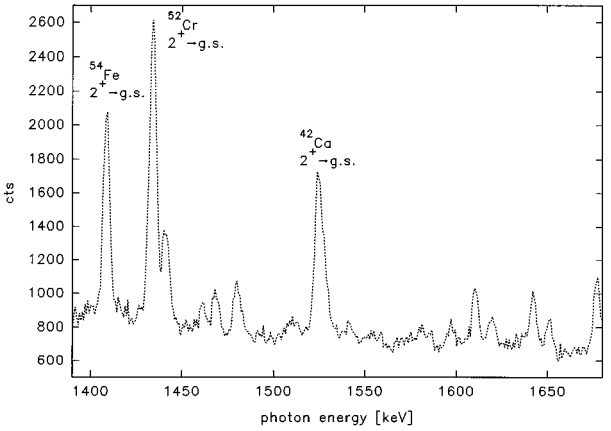

FIG. 1. Part of the prompt γ-ray spectrum from the interaction of ^{56}Fe with 800 MeV protons.

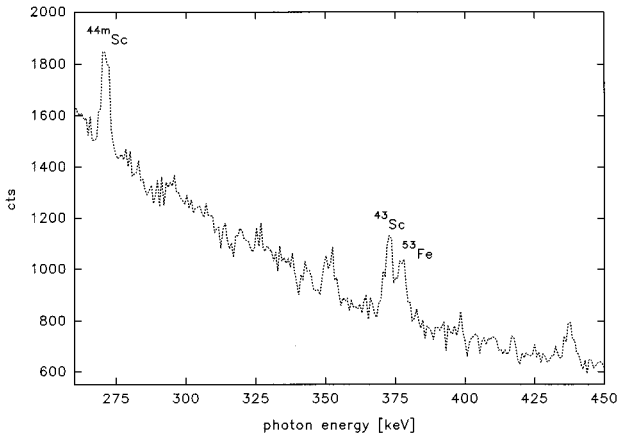

FIG. 2. Part of the delayed γ-ray spectrum from the interaction of ^{56}Fe with 800 MeV protons.

tematics of Silberberg and Tsao [3] and calculations according to the quantum-molecular-dynamics (QMD) model [4,5].

II. EXPERIMENTS

Thin foils of ^{27}Al and ^{56}Fe were irradiated with the 800 MeV proton beam of the WNR (Weapons Neutron Research) facility of the Los Alamos National Laboratory [6]. This facility is primarily used for the production of intense, pulsed beams of fast neutrons by spallation reactions of 800 MeV protons with thick Be or Ta targets. The proton beam used for this purpose can, however, also be used parasitically for the study of proton-induced reactions with thin targets. These targets can be inserted into the proton beam at a target position upstream of the neutron producing target located in a well-shielded room equipped with a number of beam holes for the observation of the reaction products. This possibility was used in our experiment and thus the measurements could be performed simultaneously with the WNR neutron physics experiments.

Targets of 6.82 ± 0.27 mg/cm^2 and 12.13 ± 0.24 mg/cm^2 were used for ^{56}Fe and ^{27}Al. This target thickness was chosen to conform with two constraints: the maximum admissible instaneous count rate in the prompt γ spectrum and negligible degradation of the proton beam quality for the neutron target by energy straggling and small-angle scattering. The target thickness was measured after the experiment by accurate measurement of the weight and area of the irradiated part of the target foil ($\sim$1 cm^2). As the target thickness was comparable to the range of the residual nuclei the targets were backed by Be stopping foils in order to avoid counting losses due to the recoiling nuclei leaving the targets.

TABLE I. Cross sections for nuclide production determined by activation from Al+800 MeV protons.

						σ (mb)				
Nuclide	$T_{1/2}$		$E\gamma$(keV)	I(%)	This work	Previous experiments			QMD	Tsao
^{26}Si	2.21	s	228	100	<0.03	-			0.16	
^{25}Na	60.0	s	389	12.8	2.7 ± 0.3	2.6 ± 0.15	600 MeV	[2]	2.78	2.75
^{24}Na	15.024	h	1368	100	10.55 ± 0.6	11.4 ± 0.35	600 MeV	[2]	12.31	8.94
						11.2 ± 0.8		[1]		
						10.9 ± 0.24		[24]		
^{22}Na	2.60	a	1274	100	14.2 ± 0.47	14.9 ± 0.2	600 MeV	[2]	12.5	11.0
						15.1 ± 1.1		[1]		
						15.0 ± 1.5		[10]		
^{23}Ne	37.6	s	439	33	1.86 ± 0.41	5.6 ± 0.3	600 MeV	[2]	1.18	2.33
^{18}Ne	1.67	s	1041	7.9	<1.7				0.05	0.82
^{23}F	2.2	s	1701	48	<0.05				0.06	0.01
^{22}F	4.23	s	1275	100	0.16 ± 0.07				0.16	0.11
^{21}F	4.32	s	350	70.6	1.89 ± 0.15				0.70	1.21
^{20}F	11.0	s	1634	100	5.59 ± 0.34	3.89 ± 0.8	590 MeV	[18]	5.47	4.82
^{20}O	13.5	s	1057	100	0.11 ± 0.07				0.09	
^{19}O	26.9	s	1357	55.8	0.43 ± 0.12	0.80 ± 0.10	590 MeV	[18]	0.34	1.04
^{14}O	70.6	s	2313	99.4	<0.11					

TABLE II. Cross sections for nuclide production from ^{56}Fe+800 MeV protons determined by activation.

Nuclide	$T_{1/2}$	E_γ (keV)	I_γ (%)	σ (mb) This work	Previous experiments	QMD	Tsao
^{56}Co	77.3 d	846.8	100	0.447±0.022	0.64±0.9 [1]	0.078	
					0.81 [15]		
^{53}Fe	8.51 m	377.9	41	1.94±0.33	2.2±0.2 600 MeV [2]	1.17	
					2.3±0.5 600 MeV [16]		
					31±8.7 600 MeV [17]		
^{54}Mn	312.3 d	834.8	100	42.6±2.0	38.8±3.0 [1]	38.0	33.3
					28.0 [15]		
					42.3±0.6 600 MeV [2]		
^{52g}Mn	5.59 d	935	94.3	6.13±1.04	10.5±0.8 [1]	7.87[a]	26.5[a]
					13.8±0.4 600 MeV [2][a]		
					14.1 [15]		
^{52m}Mn	21.1 m	1434.1	100	7.86±0.48	1.5±0.3 590 MeV [18]		
					7±0.2 600 MeV [16]		
^{50m}Mn	1.74 m	783.3	100	0.19±0.10			1.19
^{51}Cr	27.7 d	320.1	10.1	44.6±2.4	44.7±3.4 [1]	24.2	43.2
					38.5±0.6 600 MeV [2]		
					20.1 [15]		
^{49}Cr	41.9 m	152.9	31.2	11.74±0.95	3.6±0.2 600 MeV [2]	1.37	7.76
					19.4±2 590 MeV [18]		
					7.3±0.5 660 MeV [17]		
^{48}Cr	21.56 h	308	100	<0.22	0.91±0.16 [9]	0.15	1.90
^{53}V	1.6 m	1006	90	<0.33		0.72	0.50
^{48}V	15.98 d	983.5	100	25.3±1.2	23.0±1.7 [1]	13.6	22.8
					19.5±0.3 600 MeV [2]		
					4.7 [15]		
					15±2 660 MeV [17]		
^{51}Ti	5.8 m	320	93.2	<0.30		0.79	0.50
^{48}Sc	43.7 h	1037	97.8	<0.4	0.57 600 MeV [22]	0.38	0.52
					0.2±0.02 600 MeV [2]		
					0.46±0.03 590 MeV [21]		
^{47}Sc	3.42 d	159.4	68.5	<4.80	1.48 [15]	2.14	2.12
					3.28±0.24 [1]		
					2.0±0.1 600 MeV [2]		
^{46}Sc	83.8 d	889.3	100	11.2±0.52	10.7±0.8 [1]	9.37	5.96
					11.4±0.6 600 MeV [2]		
					6.4 730 MeV [13]		
					5.8±0.9 660 MeV [17]		
^{44g}Sc	3.93 h	1157	99	7.01±0.64	13±3 600 MeV [16]	18.9[a]	17.6[a]
					9±2.6 660 MeV [17]		
					17.2±0.9 600 MeV [2][a]		
^{44m}Sc	2.44 d	271.2	86.6	5.56±0.67	9.88±0.72 [1]		
					9.10 600 MeV [22]		
					5.2 [14]		
^{43}Sc	3.89 h	372.9	22	4.4±0.9	4.56 600 MeV [22]	3.16	7.6
					3±1 660 MeV [17]		
					4.3±0.2 600 MeV [2]		
^{42m}Sc	62 s	437.5	100	0.43±0.12			1.37[a]
		1227	100				
^{42}K	12.36 h	1524.6	18	4.4±1.9	3.2 730 MeV [19]	4.40	2.25
					5.6±0.03 600 MeV [2]		
					2.6±0.23 660 MeV [17]		
					2.97±0.15 660 MeV [25]		
					4.25 600 MeV [22]		
					3.02±0.31 590 MeV [21]		

TABLE II. (*Continued*).

Nuclide	$T_{1/2}$	E_γ (keV)	I_γ (%)	σ (mb) This work	Previous experiments			QMD	Tsao
					5.6±0.30	660 MeV	[2]		
^{38m}K	7.61 m	2167.6	100	0.79±0.2	0.5±0.05	600 MeV	[2]	0.38[a]	1.38[a]
^{41}Ar	1.83 h	1293.6	99.2	0.39±0.13	0.67	600 MeV	[22]	0.43	0.40
^{39}Cl	56 m	1517	40	<0.3	0.21	730 MeV	[19]	0.19	0.27
^{38}Cl	37.3 m	1642.2	31	1.17±0.32	0.83	730 MeV	[19]	1.49	0.88
					0.80±0.07	660 MeV	[17]		
^{34}Cl	32 m	2127.4	41.4	0.25±0.12	0.59	730 MeV	[19]	0.56	1.34
					0.6±0.07	660 MeV	[17]		
^{32}Cl	0.3 s	2230	92	<0.03					0.02
^{38}S	170 m	1942	84	<0.12	0.05±0.01	660 MeV	[17]	0.01	0.05
^{37}S	5.0 m	3103	94.1					0.09	0.16
^{35}P	47 s	1572	100	<0.16				0.03	0.12
^{33}Si	6.2 s	1848	81	<0.12				0.01	0.37
^{26}Si	2.21 s	228	100	<0.15					0.04
^{30}Al	3.69 s	2235	65	<0.29				0.04	0.17
^{29}Al	6.6 m	1273.3	89	0.79±0.2				0.52	0.72
^{28}Al	2.24 m	1778.7	100	2.55±0.25				2.99	1.78
^{28}Mg	21 h	400.6	36.1	<0.6	0.08±0.02	660 MeV	[17]	0.01	0.17
^{27}Mg	9.46 m	1014.5	27.2	1.0±0.4				0.22	0.44
^{25}Na	60 s	975.2	14.3	<0.80				0.07	0.33
^{24}Na	15.02 d	1368.6	100	1.66±0.19	1.07		[15]	0.54	0.90
		2754.1	100						
^{22}Na	2.60 a	1274.6	100	0.87±0.042	0.86±0.07		[1]	0.27	0.81
					0.36	730 MeV	[19]		
^{23}Ne	37.6 s	440	33	<0.3				0.02	0.21
^{20}F	11 s	1634	100	0.76±0.11				0.07	0.49

[a]Total nuclide production cross section.

The average beam current (~0.5–1 μA) was measured and registered in 1 min intervals by means of a precision inductive current measuring device to an accuracy of better than 2%.

The γ-radiation from the targets was measured with a high-purity Ge detector at a distance of about 30 m from the targets at an angle of 150° relative to the proton beam. The WNR beam consisted of 40 macropulses per s separated by either 16.66 or 33.33 ms. Each macropulse had a length of 600 μs. Within each macropulse the beam consisted of narrow micropulses of a width of about 1 ns at intervals of 1.8 μs. Accordingly the prompt γ radiation originating from the so-called γ-cascade deexciting the final residual nucleus was observed by its time correlation to the micropulses. For this purpose a two-dimensional measurement $E_\gamma - T$ was performed during the accelerator macropulses, T being the difference between time signals derived from the accelerator micropulses and the Ge-detector pulses. In this way it was possible to separate the prompt γ radiation originating from the targets from γ ratiation produced in the detector and its

TABLE III. Nuclide production cross sections derived from intensity of prompt $2_1^+ \rightarrow$g.s. transitions for Al+800 MeV protons.

Nuclide	$E\gamma$ (keV)	σ (mb) This work	Previous experiments			QMD	Tsao
^{26}Mg	1808.7	38.04±3.0	40.1±0.6	600 MeV	[2]	27.9	17.4
^{24}Mg	1368.6	29.0±2.3	27.2±0.4	600 MeV	[2]	11.7	17.6
^{22}Mg	1247	<0.5				0.18	0.74
^{20}Ne	1633.8	9.87±0.8	20.4[a]±2		[1]	9.97	14.0
			10.9±0.3	600 MeV	[2]		
^{18}Ne	1887.3	<0.05				0.05	0.82
^{20}O	1673.7	<0.20				0.09	0.09
^{18}O	1982.2	3.75±0.38				3.0	5.09

[a]Corrected for contribution from ^{20}F and ^{20}Na.

TABLE IV. Nuclide production cross sections for ^{56}Fe+800 MeV protons derived from the intensity of prompt $2_1^+ \rightarrow$g.s. transitions.

		σ (mb)				
Nuclide	$E\gamma$ (keV)	This work	Previous experiments		QMD	Tsao
^{56}Fe	846.8	23.4±2.1			2.05	
^{54}Fe	1408.4	20.2±3.5	12.2±0.4	600 MeV [2]	7.05	
^{52}Fe	840	<0.76	1.8±0.3	660 MeV [17]	0.20	
^{54}Cr	834.9	3.3±0.3	3.0±0.15	600 MeV [2]	5.75	3.7
			3.4±1	600 MeV [23]		
^{52}Cr	1431.1	44.2±2.7	40.5±0.6	600 MeV [2]	22.0	33.2
			56.1±13	600 MeV [23]		
^{50}Cr	783.3	26.5±2.4	23.7±0.4	600 MeV [2]	10.4	35.6
			27±2.8	600 MeV [23]		
^{50}Ti	1553.7	<1.2	1.2±0.12	600 MeV [2]	1.03	1.27
^{48}Ti	983.5	22.7±2.3	22.3±0.3	600 MeV [2]	12.3	13.9
^{46}Ti	889.2	32±3.8	19.6±0.3	600 MeV [2]	17.3	29.8
^{44}Ti	1083	0.94±0.53	0.78±0.06 [11]		0.18	2.01
^{46}Ca	1347	1.13±0.47			0.32	0.44
^{44}Ca	1157	9.7±1.6	8.0±0.4	600 MeV [2]	6.23	5.43
^{42}Ca	1524.6	32.7±2.9	18.5±0.3	600 MeV [2]	20.0	22.0
^{40}Ca	3730[b]	<0.1	0.5±0.05	600 MeV [2]		2.0
^{42}Ar	1208.2	<0.47	0.04±0.006	730 MeV [13]	0.05	0.14
^{40}Ar	1460.8	1.97±0.55	3.1±0.15	600 MeV [2]	2.71	1.99
^{38}Ar	2167.8	12±1.3	17.9±1.6 [1][a]		18.0	14.0
			9.7±0.3	600 MeV [2]		
^{36}Ar	1970	<1.2	1.13	600 MeV [12]	0.46	2.01
			1.1±0.1	600 MeV [2]		
^{36}S	3291	<0.3	0.9±0.1	600 MeV [2]	0.74	0.86
^{34}S	2127.4	3.8±0.3	6.1±0.1	600 MeV [2]	11.6	7.51
^{32}S	2230	<0.3	1.1±0.1	600 MeV [2]	0.55	1.80
^{32}Si	1941	<0.5	0.46	730 MeV [13]	0.18	0.37
^{30}Si	2335	<0.75			5.2	3.69
^{28}Si	1779	<0.5			0.54	1.59
^{22}Ne	1247.6	<0.7	0.8±0.15 [14]		0.20	0.94
			0.4	600 MeV [12]		
^{20}Ne	1633.8	<0.6	0.75	600 MeV [12]	0.10	1.13
			1.04±0.2 [14]			
^{14}O	1982.2	<0.75			0.03	0.65

[a]Corrected for contribution of ^{38}Cl and ^{38}K according to Ref. [9] and this work.
[b]Energy of lowest 3^- level.

surroundings by the neutrons also produced in the targets.

The γ radiation from the decay of the short-lived residual nuclei formed in spallation reactions was measured between the macropulses by setting a time window of 15 ms after the end of each macropulse. Two runs, each of about 1 day duration, were performed for each target.

The efficiency of the Ge detector was measured (using the same time windows as in the experiments) to about ±3% by means of calibrated sources of ^{152m}Eu and ^{56}Co over the energy range 0.12–3.5 MeV. The calibration measurement was performed at a source to detector distance of 64 cm. The efficiency measurement was transformed to the target-detector distance of 30 m employed in the experiment using the inverse square law and an appropriate correction for photon attenuation in the air of the flight path. Examples of the raw data are given in Figs. 1 and 2 showing parts of the prompt and delayed spectra from the interaction of the protons with ^{56}Fe. The number of counts in the gamma peak areas was obtained by adding the channel contents within the peak and subtracting a smooth background. This background was obtained from a linear fit to suitable background regions on both sides of the peak. After the experiment the irradiated Al and Fe foils were transferred to the Institut für Radiumforschung und Kernphysik, University of Vienna and the γ-radiation from all long-lived activities produced in the samples was measured with a high-purity Ge detector calibrated to better than 2%.

III. DATA ANALYSIS

As the main purpose of this work is determination of the mass and charge distribution of the spallation products, the

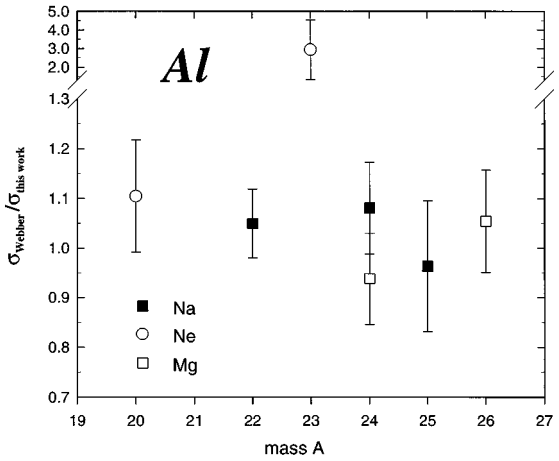

FIG. 3. Comparison of our data for Al with the results of Webber [2] from direct observation of recoils. Open squares=Mg, closed squares=Na, open circles=Ne.

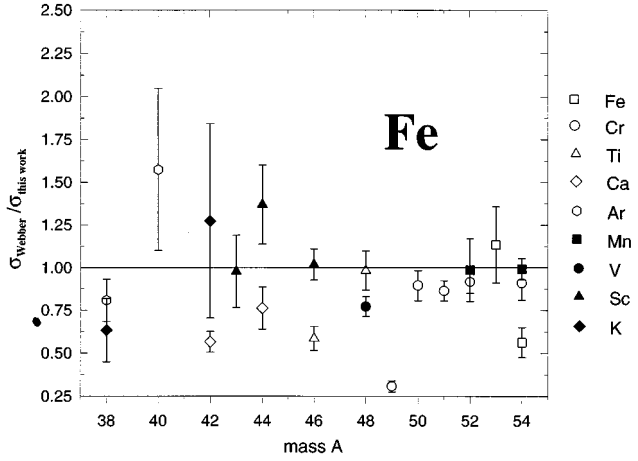

FIG. 4. Comparison of our data for ^{56}Fe with the results of Webber [2] observed by direct observation of recoils. Open squares=Fe, closed squares=Mn, open circles=Cr, closed circles=V, open triangles=Ti, closed triangles=Sc, open diamonds=Ca, closed diamonds=K, open hexagons=Ar.

analysis of the prompt spectra was restricted to the measurement of the cross sections for transition from the first excited 2^+ levels to the ground state in even-even nuclei as only these can be directly converted into production cross sections for the corresponding residual nuclei. From reactions at lower incident energies it is well known that more than 90% of all γ cascades in even-even nuclei proceed via this transition as the last step of the cascade. At our incident energy of 800 MeV this fraction will be even higher because of the larger average spin of the residual nuclei at the beginning of the γ cascade. In addition it has been shown that the angular distributions of these $2^+ \rightarrow$ ground state (g.s.) γ lines become nearly isotropic above incident energies of some 100 MeV [7]. Therefore it can be safely assumed that the relative intensities of γ lines from $2_1^+ \rightarrow$ g.s. transitions observed at one angle (150°) can be used as relative cross sections for the formation of the corresponding residual nuclei. In the prompt Al spectra the density of γ lines is sufficiently low so that chance coincidences between the energies of the $2_1^+ \rightarrow$ g.s. transitions in question and other strong γ lines are highly improbable. In the case of the prompt ^{56}Fe spectra a much larger number of residual nuclei contributes with comparable intensity and it has to be checked carefully whether the energies of the considered $2_1^+ \rightarrow$ g.s. transitions coincide within our energy resolution (3 keV) with the energies of other strong γ transitions. For this purpose all γ transitions occurring within the lowest 20 levels of all residual nuclei produced with noticeable cross sections were extracted from the ENSDF file [8] and combined into one list ordered by γ energy. This list was used to check all considered γ lines for ''contaminations.'' In this search we identified four such cases. The 1408.4 keV, $2_1^+ \rightarrow$ g.s. transition in ^{54}Fe cannot be resolved from the 1408.5 keV $(\frac{7}{2})_1^+ \rightarrow$ g.s. transition in ^{55}Fe and the 889.2 keV $2_1^+ \rightarrow$ g.s. transition in ^{46}Ti is ''contaminated'' by the 891.6 keV γ line from the $5_1^- \rightarrow$ g.s. transition in ^{40}K. In both cases estimated corrections (amounting to $\sim$20%) were applied to our measured peak intensities. In addition the 1807.7 and 1368.7 keV $2_1^+ \rightarrow$ g.s. in ^{26}Mg and ^{24}Mg transitions cannot be resolved from transitions at 1810.8 keV (in ^{56}Fe) and 1369.7 keV (in ^{55}Fe). As the expected intensities of the interfering lines are comparable to the total observed peak intensities no determination of the ^{24}Mg and ^{26}Mg production cross section was possible. In order to convert the relative values into absolute cross sections for the Fe experiment we combined our accurate activation cross section measurement for ^{51}Cr (44.59 $\pm$2.36 mb, see Table II)[1] with the production ratio $\sigma_{^{52}\mathrm{Cr}}/\sigma_{^{51}\mathrm{Cr}}=1.052$ determined in [2]. Because of the small mass difference and the fact that both nuclides are in the flat peak of the mass distribution this ratio is to a large extent free of systematic errors and accurate to about 3%. Combining these two values we obtain a value of 44.2$\pm$2.7 mb for ^{52}Cr and the cross sections for all other even-even nuclei were calculated by means of the relation

$$\sigma_A(\mathrm{mb}) = 44.2 \, \frac{N_A}{N_{^{52}\mathrm{Cr}}} \, \frac{\varepsilon_{1.43}}{\varepsilon_{E_A}}. \qquad (1)$$

N_A is the number of counts in the γ-peak from the $2_1^+ \rightarrow$ g.s. transition from nuclide A, $N_{^{52}\mathrm{Cr}}$ is the number of counts in the 1.43 MeV peak from the $2_1^+ \rightarrow$ g.s. decay in ^{52}Cr.

In the calculation of the uncertainties the statistical uncertainties of N_A and $N_{^{52}\mathrm{Cr}}$, the stated error of the reference cross section and the uncertainty of the efficiency ratio $\varepsilon_{1.43}/\varepsilon_{E_A}$ (3%) were added quadratically. In addition, an uncertainty of 3% was added for possible differences in angular distribution of the transition in ^{52}Cr and nuclide A, and 5% for possible differences in the fraction of the residual nuclei decaying via $2_1^+ \rightarrow$ g.s transitions in ^{52}Cr and nuclide A.

[1]Reduced by 6% in order to correct for the contribution of ^{51}Mn to the measured ^{51}Cr activity [2].

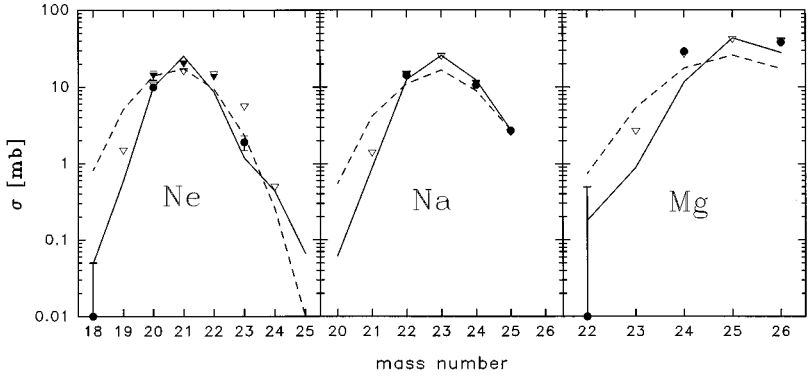

FIG. 5. Independent production cross sections for Mg, Na, and Ne isotopes in the interaction of 600–800 MeV protons with Al. Closed circles: this work, open triangles: Webber [2], closed triangles: Michel [1], closed diamonds: other experiments, solid line: QMD calculation, dotted line: Tsao-Silberberg systematics.

For the ^{27}Al experiment we normalized our cross sections to the weighted average of the ^{22}Ne cross section measured by Webber *et al.* [2] 14.9 ± 0.78 mb and Michel *et al.* [1] 13.8 ± 0.88 mb. Accordingly, the cross sections were calculated by means of the relation

$$\sigma_A(\text{mb}) = 14.4 \frac{N_A}{N_{^{22}\text{Ne}} \varepsilon_{E_A}} \frac{\varepsilon_{1.274}}{}. \tag{2}$$

The uncertainties of these values were calculated as described before.

The γ-intensities observed in the delayed spectra were converted into nuclide production cross sections by means of the relation

$$\sigma(\text{mb}) = 10^{27} \frac{N(E_\gamma)}{\varepsilon(E_\gamma)} \frac{(r_1/r_2)^2 1.602 \times 10^{-16} \exp(\mu r_1)}{Q(nd) f_T B} \tag{3}$$

with $N(E_\gamma)$ the number of counts in the γ peak, ε the peak efficiency for E_γ, r_1, r_2 the source detector distances in the experiment (30.06 m) and in the calibration run (0.641 m), Q the integrated charge of the experiment in mC, nd the target thickness (nuclei/cm^2), B the branching ratio of the observed γ line in the investigated decay, $\exp(\mu r_1)$ the correction for the γ attenuation of the air between target and detector (not present in the calibration experiment), and f_T the fraction of all decays occurring during the measurement.

The factor f_T depends on the half-life $T_{1/2}$ of the respective decay, the irradiation time T_{irr}, and the time dependence of the proton intensity during the irradiation and during all irradiations of the investigated target preceding the considered measurement. It can be calculated analytically for the case of constant proton intensity. In our experiments this approximation was not applicable due to a number of intermissions within each run and other fluctuations of the beam current intensity. Therefore a computer code was developed to calculate f_T. In this code the whole irradiation time, that is the time between the first irradiation of the considered target to the end of the considered measurement, is divided into a large number of time intervals. For each interval the code calculates the fraction Q_i/Q of the total charge delivered within the interval ΔT_i and the fraction $f(\Delta T_i)$ of all nuclei formed in ΔT_i which decay during the considered measuring time. Finally the fraction f_T is calculated:

$$f_T = \sum_i \frac{Q_i}{Q} f(\Delta T_i). \tag{4}$$

The cross-section uncertainties were calculated by quadratic addition of the uncertainties of all factors in Eq. (3). Uncertainties of about 3% were estimated for $(r_1/r_2)^2$, $\varepsilon(E_\gamma)$, and Q, respectively, uncertainties of 2 and 4 % were assigned to the target thickness (nd) of Al and ^{56}Fe and the uncertainties of f_T and $\exp(\mu r_1)$ can be neglected.

For radioactive residual nuclei decaying into stable nuclei we had to deal with the additional complication in cases where the same level of final stable nuclei is populated by both β^- and β^+, respectively, EC, decays. In these cases assignment of the observed γ intensities was either based on γ lines populated only in one of the decays allowing to split the jointly populated γ lines into their components or, if no such lines existed, on the already existing information on the mass and charge distribution, which in most cases allowed to neglect the contribution of one of the decays relative to the other. The same problem occurred for decays from isomer and ground states of residual nuclei. Due to the spin differences between these levels, however, some γ rays are populated in only one of the decays and a determination of both cross sections was possible.

After the irradiation the Al and Fe samples were transferred to the Institut fur Radiumforschung und Kernphysik in

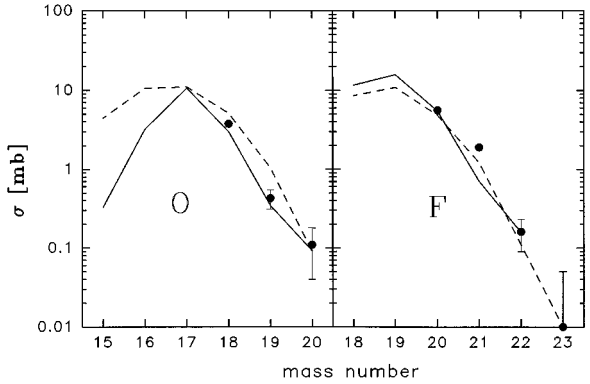

FIG. 6. Independent production cross sections for O and F isotopes from the interaction of 600–800 MeV protons with Al. The notation is the same as in Fig. 5.

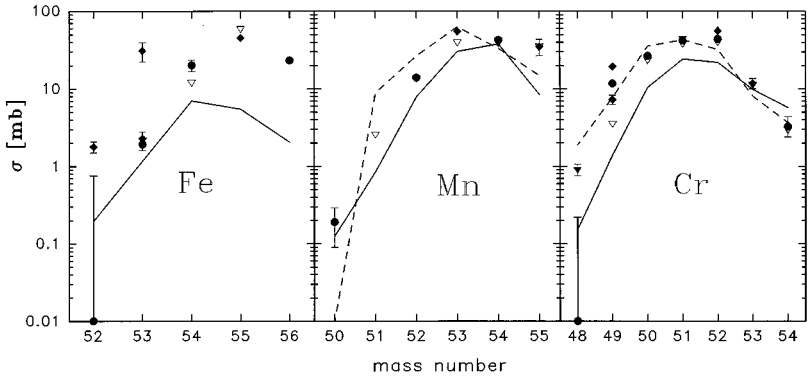

FIG. 7. Independent production cross sections for Fe, Mn, and Cr isotopes from the interaction of 600–800 MeV protons with ^{56}Fe. The notation is the same as in Fig. 5.

Vienna and the activity of long-lived residual nuclei (^{56}Co, ^{54}Mn, ^{51}Cr, ^{48}V, ^{46}Sc, and ^{22}Na) was measured with a calibrated high-purity Ge γ-ray detector. The uncertainty of the efficiency calibration of this detector was less than 2%. For every nuclide the most intense γ lines were analyzed as described above and the production cross sections were derived from the measured activities.

IV. RESULTS AND DISCUSSION

The results of the activation measurements for both the short- and long-lived residual nuclei and the decay data used in the determination of the cross sections are summarized in Tables I and Tables II and compared to all previous data [1,2,9–25]. The tables include all reported cross section data at $E = 800$ MeV, the cross sections from direct observation of the recoiling nuclei [2] and a number of activation measurements in the energy range 590–800 MeV, as most cross sections are approximately constant (within about 10–20 %) over this energy range [1,2,3,4,26]. Cases in which the incident energy of the literature values is different from the energy of this work are specially marked in the tables. Furthermore the tables give the predictions of the semiempirical systematics of Tsao and Silberberg [3] and of the QMD model [4]. The cross sections for formation of even-even nuclei from the prompt γ spectra are shown in Tables III and Tables IV where they are compared to both existing measurements and theoretical predictions in the same way as described for Tables I and II.

As apparent from Tables I and II, there is excellent agreement between our activation measurements for long-lived residual nuclei (^{54}Mn, ^{51}Cr, ^{48}V, ^{46}Sc, and ^{22}Na) with the recent results of Michel *et al.* [1] and strong disagreement with the older activation measurements [13,15,17]. These older experiments seem to suffer from some systematic error, such as inadequate consideration of the effects of secondary particles. Concerning the cross sections of [1] for production of noble gases by mass spectroscopy, our data show some significant discrepancies for the production of ^{20}Ne from Al (see Table I) and ^{38}Ar from ^{56}Fe (see Table IV). In both cases our data for the production of these nuclei agree with the results from Webber *et al.* [2].

As discussed in [1], there exist considerable discrepancies between the data of their work from activation, conventional and accelerator mass spectroscopy and the results of [2] from direct observation of the recoiling residual nuclei, which need further clarification. A comparison of our data with those of [2] is therefore shown in Figs. 3 and 4. The figures show the ratio between the cross sections of [2] and our present measurements; the uncertainties of the ratios are derived from the cross section uncertainties listed in Tables I–IV.

Figure 3 and Tables I and III show that there is agreement within experimental uncertainties between our results and those of [2] for the Al experiment except for the case of ^{23}Ne. There, our result is much smaller than that of [2]. For the ^{56}Fe experiment the situation is less satisfactory (see Fig. 4 and Tables II and IV). For 4 out of 19 residual nuclei the cross-section ratios deviate from unity far outside of the estimated uncertainty. For the three cases ^{54}Fe, ^{46}Ti, and ^{42}Ca our cross sections derived from the prompt $2_1^+ \rightarrow$g.s. intensity are about a factor of 1.7 higher than Webber's result and the cross section for formation of ^{49}Cr determined by activation was found to be three times larger than given in [2]. The discrepancies for ^{54}Fe, ^{46}Ti, and ^{42}Ca could, in principle, be due to γ lines coinciding in energy with the

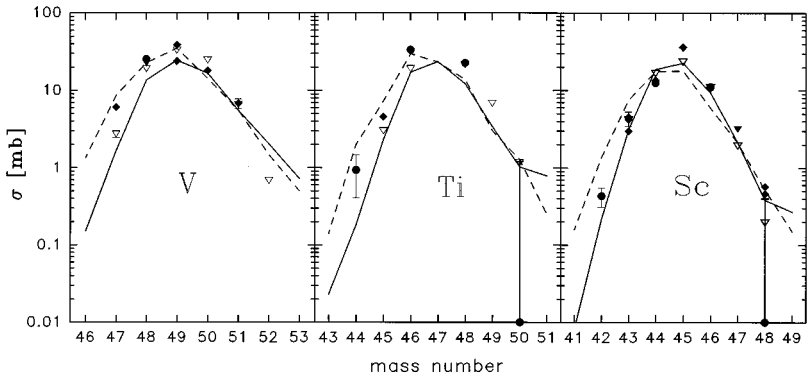

FIG. 8. Independent production cross sections for V, Ti, and Sc isotopes from the interaction of 600–800 MeV protons with ^{56}Fe. The notation is the same as in Fig. 5.

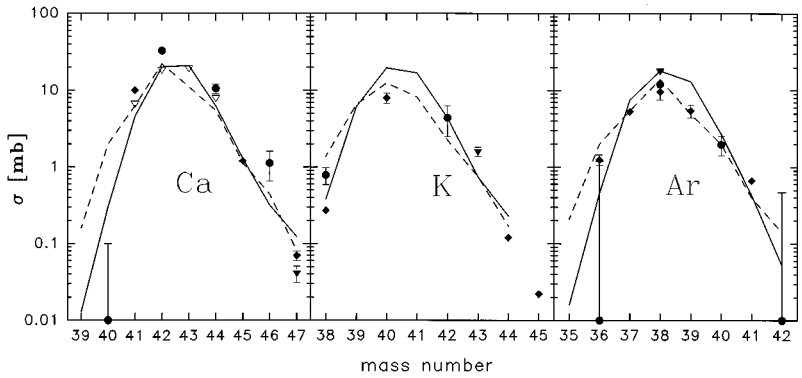

FIG. 9. Independent production cross sections for Ca, K, and Ar isotopes from the interaction of 600–800 MeV protons with ^{56}Fe. The notation is the same as in Fig. 5.

respective $2_1^+ \rightarrow$g.s. transitions in our spectra, but the occurrence of three such cases with rather high cross sections seems highly improbable considering our careful check for such contaminating transitions. In the case of ^{49}Cr, which was measured by activation in our experiment, we do not see how we could overestimate the cross section by a factor of 3. In addition, previous activation measurements on ^{49}Cr production (see Table II) also give much higher cross sections than [2]. Finally it is to be noticed that also some upper limits derived from our data for cross sections in the wings of the mass distribution also disagree with the results of [2]. On the whole, however, our data show a somewhat better agreement with the data of Webber *et al.* [2] than observed by Michel *et al.* in the comparison of his data to [2] (see Fig. 14 of [1]).

The experimental situation can be summarized as follows: A considerable part of the older activation measurements has proved unreliable and should no longer be considered for comparison with theory. However, even the three most recent and most complete sets of cross section measurements for aluminum and iron, [1,2] and this work, do show some disturbing discrepancies between each pair of experiments which need further clarification. In detail new measurements should be performed to resolve the discrepancies concerning ^{20}Ne and ^{23}Ne production from aluminum and production of ^{54}Fe, ^{49}Cr, ^{46}Ti, ^{42}Ca, and ^{38}Ar from iron and also new measurements on production of sulfur and silicon isotopes in order to check the very low cross sections for these isotopes indicated by our results (see Table II).

A comparison of all existing data on spallation of aluminum and iron with the semiempirical systematics of Tsao and Silberberg [3] and the quantum-molecular-dynamics model (QDM) followed by statistical decay (SDM) is given in Figs. 5–10 showing the nuclide production cross sections for O-Mg from Al and Ar-Fe from ^{56}Fe. All calculations were performed for an incident proton energy of 800 MeV. The calculations according to the Tsao systematics were performed using a special version of the code SPALL [9] incorporating the most recent features of the Tsao systematics and were supplied to us by Michel [27]. The QMD+SDM model [4,5] has evolved from the intranuclear cascade model (INC). It differs from the conventional INC (as, e.g., used in the code HETC) mainly by introducing a self-consistent mean-field effect which results in the formation of complex particles already in the first cascade stage of the reaction [4,5]. For the case of the reaction considered it seems to be equivalent to the conventional INC model. Experimental data shown cover the energy range 590–800 MeV where the cross section is expected to change by less than about 15% [1,3,26]. In this way a much larger data base can be used for the comparison at the expense of a relatively small additional uncertainty, as both the differences between measurements and theory and within the different measurements are considerably larger than the effect of different incident proton energies in the chosen mass range. All calculated cross sections in Figs. 5–10 are independent cross sections, the same is true for the results of direct observation of recoils [2] and our results derived from the prompt γ spectra. All cross sections derived from activation measurements and mass spectrometry were therefore also converted to independent cross sections by suitable corrections for the production of the respective nuclei by radioactive decay of neighboring nuclides. Points with one-sided error bars sitting on the abscissa indicate upper limits for cross sections obtained in this work.

Figures 5 and 6 show that for Al the quality of the theoretical description by the QMD model is now approximately as good as that of the semiempirical systematics, although the QMD model does not contain any parameters fitted to the existing data on nuclide production cross sections.

For ^{56}Fe (Figs. 7–10) the QMD model does not quite so well. In this case the model seems to systematically underestimate the production of nuclides with low ΔZ and to overestimate the production of higher ΔZ values and does not

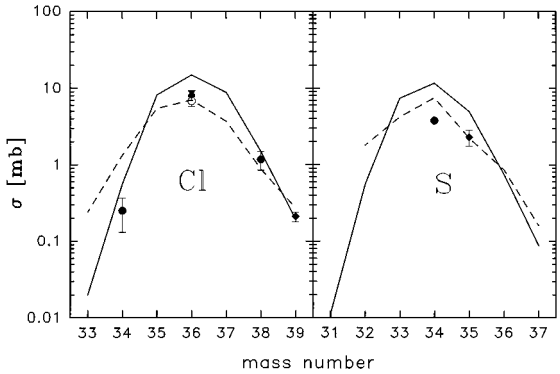

FIG. 10. Independent production cross sections for Cl and S isotopes from the interaction of 600–800 MeV protons with ^{56}Fe. The notation is the same as in Fig. 5.

give a description as good as the systematics.

However, there are for both targets still deviations up to a factor of 2 between the experimental data and both calculations even for nuclides in the peaks of the mass distribution. Unfortunately the overall spread even of the more recent data is still so large that it is difficult to draw general conclusions on possible systematic dependencies of the observed discrepancies on Z and A.

ACKNOWLEDGMENTS

This work was supported by the Austrian Fonds zur Förderung der wissenschaftlichen Forschung (Project P9587-PHY). The authors also gratefully acknowledge the support from Dr. R. Michel, University Hannover, who supplied to them the most recent results of the Tsao-Silberberg systematics.

[1] R. Michel *et al.*, Nucl. Instrum. Methods Phys. Res. B **103**, 183 (1995), and references therein.
[2] W. R. Webber, J. C. Kish, and D. A. Schrier, Phys. Rev. C **41**, 547 (1990).
[3] R. Silberberg and C. H. Tsao, Astrophys. J. **220**, 315 (1973); **220**, 335 (1973); R. Silberberg, C. H. Tsao, and M. M. Shapiro, in *Spallation Nuclear Reactions and Their Applications*, edited by B. S. P. Shen and M. Merker (Reidel, Dordrecht, 1976), p. 49; C. H. Tsao and R. Silberberg, *Proceedings of the 16th International Cosmic Ray Conference*, Kyoto (University of Tokyo, Tokyo, 1979), Vol. 2, p. 202; R. Silberberg, C. H. Tsao, and J. R. Letaw, Astrophys. J. Suppl. Ser. **58**, 873 (1985); R. Silberberg, C. H. Tsao, and J. R. Letaw, *Proceedings of the 20th International Cosmic Ray Conference*, Moscow (Nauka, Moscow, 1987), Vol. 2, p. 133; R. Silberberg, C. H. Tsao, J. H. Adams, and J. R. Letaw, *High Energy Radiation Background in Space*, edited by A. C. Rester, Jr. and J. J. Tombka, (AIP Conf. Proc. No. 186, New York, 1989), and references therein.
[4] K. Niifa *et al.*, Phys. Rev. C **52**, 2620 (1995).
[5] S. Chiba *et al.*, Phys. Rev. C **54**, 285 (1996).
[6] P. W. Lisowski, C. D. Bowman, G. J. Russell, and S. A. Wender, Nucl. Sci. Eng. **106**, 208 (1990).
[7] R. O. Nelson, S. A. Wender, and D. R. Mayo, in *Proceedings of a Specialists' Meeting on Measurement, Calculation and Evaluation of Photon Production Data*, Bologna, Italy, 1994, edited by C. Coceva, A. Mengoni, and A. Ventura [Nuclear Energy Agency Report No. NEA/NSC/DOC(95)1, 1995], p. 281.
[8] ENSDF, The Evaluated Nuclear Structure Data File, Data received from IAEA, Nuclear Data Section, Vienna, 1996.
[9] M. Lüpke, Ph.D. Thesis, Universität Hannover, 1993.
[10] H. R. Heydegger, A. L. Turkevich, A. van Ginneken, and P. H. Walpole, Phys. Rev. C **14**, 1506 (1976).
[11] S. Ohnimus, Diplomarbeit, Universität Hannover, 1990.
[12] K. Goebel, H. Schultes, and J. Zahringer, ''Production Cross Sections of Tritium and Rare Gases in Various Target Elements,'' CERN Report No. CERN-64-12, 78, 1964.
[13] M. Honda and D. Lal, Nucl. Phys. **51**, 363 (1964).
[14] F. Baros and S. Regnier, J. Phys. (France) **45**, 855 (1984).
[15] G. V. S. Rayudu, J. Inorg. Nucl. Chem. **30**, 2311 (1969).
[16] J. E. Cline, E. B. Nieschmidt, R. J. Gehrke, E. L. Murri, and L. D. McIsaac (unpublished).
[17] A. K. Lavrukhina, L. P. Moskaleva, V. V. Malyshev, and L. M. Satarova, Sov. Phys. JETP **16**, 1 (1963).
[18] J. E. Cline and E. B. Nieschmidt, Nucl. Phys. **A169**, 437 (1971).
[19] M. Honda and P. Lal, Phys. Rev. **118**, 1618 (1960).
[20] R. L. Brodzinski, L. A. Rancitelli, J. A. Cooper, and N. A. Woyman, Phys. Rev. C **4**, 1257 (1971).
[21] C. J. Orth, H. A. O'Brien, M. E. Schillaci, and B. J. Dropesky, J. Inorg. Nucl. Chem. **38**, 13 (1976).
[22] B. J. Dropesky and H. A. O'Brien, Los Alamos Scientific Lab. Report No. LA-5120-PR, 1972.
[23] C. Perron, Phys. Rev. C **14**, 1108 (1976).
[24] J. B. Cumming, V. Agoritsas, and R. Witkover, Nucl. Instrum. Methods **180**, 37 (1980).
[25] M. Lagarde-Simonoff, S. Regnier, H. Sauvageon, G. N. Simonoff, and F. Brout, J. Inorg. Nucl. Chem. **37**, 627 (1975).
[26] W. R. Webber, J. C. Kish, and D. A. Schrier, Phys. Rev. C **41**, 533 (1990).
[27] R. Michel, private communication.